The isotopic composition of volatiles in the unique Bench Crater carbonaceous chondrite impactor found in the Apollo 12 regolith

Katherine H. Joy, Romain Tartèse, Scott Messenger, Michael E. Zolensky, Y. Marrocchi, David R. Frank, David A. Kring

The isotopic composition of volatiles in the unique Bench Crater carbonaceous chondrite impactor found in the Apollo 12 regolith

K. H. Joy[1,2,*], R. Tartèse[1], S. Messenger[3], M. E. Zolensky[2,4], Y. Marrocchi[5] , D. R. Frank[4,6], and D. A. Kring[2.]

[1]Department of Earth and Environmental Sciences, School of Natural Sciences, The University of Manchester, Oxford Road, Manchester, M13 9PL, UK.

[2]Center for Lunar Science and Exploration, The Lunar and Planetary Institute, 3600 Bay Area Blvd., Houston, Texas, 77058, TX, 77204-5007, USA.

[3]Previously based at Robert M Walker Laboratory for Space Science, Astromaterials Research and Exploration Science, NASA Johnson Space Center, Houston, TX 77058, USA.

[4]XI2, Astromaterials Research and Exploration Science, NASA Johnson Space Center, Houston, TX 77096, USA.

[5]CRPG, CNRS, Université de Lorraine, UMR 7358, Vandoeuvre-les-Nancy, F-54501, France

[6]now based at University of Hawai'i at Manoa Hawai'i Institute of Geophysics and Planetology 1680 East-West Road, POST 602, Honolulu, HI 96822 USA

[*]Corresponding author: Katherine.Joy@manchester.ac.uk.

Abstract

Projectiles striking the Moon have modified its crust and delivered volatile elements to its interior and surface. Direct evidence of impactor origins is recorded by the rare occurrence of sub-cm sized meteorite fragments identified in Apollo samples and lunar meteorites. The Bench Crater meteorite is a millimetre-sized carbonaceous chondrite collected in regolith on the rim of Bench impact crater at the Apollo 12 landing site. Transmission electron microscopy has previously shown that Bench Crater contains abundant hydrated silicates, establishing the survivability of hydrated material impacting the lunar surface. To provide further information on the volatile inventory of the Bench Crater meteorite, we report here the isotope compositions of hydrogen, nitrogen, carbon and oxygen. This is the first direct isotopic analysis of meteoritic material delivered to the lunar surface and provides context for volatile and organic element signatures in lunar regolith samples, and the survivability of volatile material delivered to planetary surfaces during impact bombardment. The Bench Crater meteorite is characterised by δD values ranging between -36 ± 40 and 200 ± 40 ‰, and bulk average $\delta^{13}C$ of -13 ± 30 ‰, and $\delta^{15}N$ of -40 ± 36 ‰ (all uncertainties at the 2σ confidence level). The oxygen isotope compositions measured *in situ* in matrix silicates and magnetite in Bench Crater are consistent with those measured in matrix and magnetite in CI and CM chondrite falls. Altogether, these new H, C, N and O isotope data, coupled to mineralogical and geochemical observations, suggest that Bench Crater may have been derived from an asteroidal parent body not represented in the terrestrial meteorite collection. This is a crucial outcome in the current context of sample-return missions to carbonaceous asteroids, and more broadly for investigating the flux of material delivered to the Earth-Moon system through time.

Keywords: Moon, Meteorite, Light stable isotopes, Regolith, Volatiles, Carbonaceous chondrite

1. Introduction

A key driver of future lunar scientific exploration is to determine the source(s) of water ice and volatiles found on the Moon's surface at the present day (Li *et al.,* 2018), and to understand past origins of water and volatiles in the Earth-Moon system (NRC, 2007). Potential caches of water and other volatiles at the lunar surface are being targeted by spacecraft missions for both scientific and exploration objectives (*e.g.,* Carpenter *et al.,* 2014; Colaprete *et al.,* 2016; Barber *et al.,* 2017). Such volatile reservoirs at the lunar surface are of key astrobiological interest (Cockell, 2010; Martins *et al.,* 2013) and may also prove to be useful for *in situ* resource utilisation (Anand *et al.,* 2012) for the next generation of lunar surface exploration.

Over the past decade, laboratory measurements of hydroxyl and water locked in volcanic picritic glass beads and melt inclusions they host, in the phosphate mineral apatite, and in nominally anhydrous minerals have also allowed investigation of the diversity and budgets of volatile reservoirs in the lunar interior (see McCubbin *et al.,* 2015 for a review). Lunar surface volatile budgets have been constrained by spectral identifications of OH bound in regolith soils (e.g., Pieters *et al.,* 2009), concentrations of volatiles within the regolith of permanently shadowed polar craters (e.g., Colaprete *et al.,* 2009), and in Apollo regolith glasses and impact breccias (e.g., Liu *et al.,* 2012). However, the origin of these different reservoirs is poorly constrained: they are likely a mixture of both indigenous and exogenous sources (e.g., McCubbin *et al.,* 2015 and references therein; Barnes *et al.,* 2016).

Unravelling the geochemical and isotopic records of volatiles at the lunar surface is complicated by (i) limited direct measurements of end-member compositions (*i.e.* impactor types, solar wind-derived volatiles, and interior sources), (ii) few complete volatile inventory analyses of lunar soil and regolith samples (Steele *et al.*, 2010; Liu *et al.*, 2012; Stephant and Robert, 2014; Füri and Marty, 2015; Füri *et al.*, 2012, 2017, 2018; Curran et al., 2020), and (iii) complications with calculating isotopic contributions from spallogenically-derived components (e.g., Stephant and Robert 2014; Füri *et al.*, 2017). To address the first of these challenges, we have determined the isotopic composition of the volatile elements hydrogen, carbon, nitrogen and oxygen in a carbonaceous chondrite meteorite fragment from the Moon. This study, therefore, provides the first ground-truth for the composition of asteroid-derived volatiles hosted by the lunar regolith.

2. Sources of lunar impactors

The types of meteoritic material that are recovered today on the Earth (e.g., The Meteoritical Bulletin, 2020) might also be representative of the sources of material striking the Moon, contributing to the addition of volatiles to the lunar regolith. There are, however, two significant knowledge gaps preventing us from making this assessment. Firstly, weakly consolidated – and likely the most volatile-rich – meteorites (and micrometeorites) are largely contaminated (especially volatile elements) or destroyed during descent through the Earth's atmosphere and are poorly sampled, or unavailable in the Earth's meteorite collection (Trigo-Rodriguez and Blum, 2009; Flynn *et al.*, 2017). Thus, knowledge of their contribution to the meteoritic volatile inventory is incomplete. Secondly, the flux and nature of meteoritic debris may have changed with time with the dynamical evolution of small bodies in the Solar System, and meteoritic fragments found in the lunar regolith provide us with a complementary and often older record compared to terrestrial meteorites (Joy *et al.*, 2016;

Heck *et al.,* 2017). To address both of those existing shortcomings we need to examine the Moon's surficial regolith for volatile-rich meteoritic relics (Joy *et al.,* 2012 and references therein). Retention of such projectile material at the lunar surface depends upon impact velocity, impact angle, and impactor and target material properties including strength and porosity (Avdellidou *et al.,* 2016). Theoretical calculations indicate that asteroids deliver the majority of lunar near-surface volatiles compared with cometary dust particles (Svetsov and Shuvalov, 2015). To date, all impactor debris found on the Moon have been very small, ranging from a few microns to only a few mm in size (see summary in Joy *et al.,* 2016), yet provide a vital ground-truth for characterisation of volatile resources by future *in situ* mission analysis of the lunar regolith, and samples returned to the Earth.

3. Geological setting and characteristics of the Bench Crater meteorite

In this study, we characterised the petrography, mineralogy and geochemistry of a fragment of the Bench Crater carbonaceous chondrite meteorite (McSween, 1976; Fitzgerald and Jones, 1977; Zolensky *et al.,* 1996; Zolensky, 1997) (Fig. 1). The meteorite was identified from a range of small (0.6 to 3 mm) rock particles extracted from soil sample 12037 (Fig. S-1), collected from the rim of a 75 m impact crater on the nearside of the Moon at the Apollo 12 landing site (3.01°S 23.4°W) (Figs. S-2 and S-3, and Supplementary Information note 1).

The 12037 bulk soil is sub-mature, meaning that it underwent medium levels of solar wind exposure at the lunar surface compared with other Apollo soil samples (the sample has an I_s/FeO soil maturity index value of 21; Morris *et al.,* 1983). The duration of exposure of this 12037 soil to the space environment has been estimated to be 10-20 Myr based upon the density of cosmic ray tracks and nitrogen spallation ages (Arrhenius *et al.,* 1971; Becker and Clayton, 1978). This exposure age is younger than the proposed Apollo 12 landing site Bench

impact crater formation episode, thought to be ~<99 Ma (Arvidson *et al.*, 1975) and likely <55 Ma (Burnett et al., 1975). It may be that the Bench Crater meteorite represents part of the impactor that made this crater, but it may also have been delivered after this event. In any case, the Bench Crater meteorite likely impacted the Moon's surface in the last 100 million years.

4. Methods

Key aspects of the methods are described here and a full description of methodology is outline in Supplementary Materials note 2. Small pieces of the Bench Crater meteorite in section 12037,188 were removed (Fig. S-1) with a needle. Microtomed sections were prepared and analysed using the NASA Johnson Space Center (JSC) JEOL 2200FS field emission gun (FEG) transmission electron microscope (TEM) coupled to an Oxford energy-dispersive X-ray (EDX) spectroscopy system to check the presence of hydrated phases (Supplementary note S-2.2) and determine the composition of matrix materials (Table S-1). Two 15 × 15 μm areas (Area 1 and Area 2) of fragments pressed into gold foil were spatially mapped for H, C, and N isotope compositions and two 10 × 10 μm areas (Area 3 and 4) were spatially mapped for their H isotope composition in separate sessions using the NASA JSC NanoSIMS 50L ion microprobe (Table 1 and Supplementary note S-2.4).

After removing a small sub-split of the sample for NanoSIMS work, we also analysed the whole polished grain mount of Bench Crater using the NASA JSC JEOL 7600f FEG scanning electron microscope (SEM) to collect backscatter electron (BSE) images and X-ray element maps as shown in Figure 1 (Supplementary note S-2.1). Normalised phase modal proportions (Table S-2) were estimated by combining these element maps and using Adobe Photoshop to count the number of pixels in each assigned phase type. Further BSE imaging

was carried out using a FEI Quanta 650 FEG-SEM at the University of Manchester, and mineral compositions were acquired using a Cameca SX 100 electron microprobe at the University of Manchester (Table S-3).

Finally, we measured the oxygen isotopic compositions of silicates, magnetite and carbonate *in situ* in the Bench Crater meteorite thin section using a CAMECA IMS 1270 E7 at CRPG-CNRS (Nancy, France). Details are provided in Supplementary note S-2.3 and the data are listed in Table 2. After the analyses, all the SIMS spots were carefully checked by BSE-SEM to estimate potential contribution by adjacent minerals (Figs. S-7 and S-8).

5. Results and interpretation

5.1. Petrography

The Bench Crater meteorite is 3.00 × 1.75 mm in size (Fig. 1 and Fig. S-1). Transmitted light optical microscope observations show that the meteorite appears very well preserved with a low-level petrofabric (preferred matrix cross-cutting fracture orientation, see Fig. 1), sub-rounded magnetite grains, see Fig. 2) and fractured sulphides. It is composed of brown-coloured aggregates of ferromagnesian minerals that are possibly aqueously altered chondrules (olivine + pyroxene, ~10% by area of the meteorite; Fig. 3) embedded within a fine-grained matrix (~68% by area; Fig. 3). Many ferromagnesian phases in the matrix have been replaced by the hydrated mineral saponite (with a chemical composition of $Ca_{0.01}Mg_{0.06}(Mg_{2.73}Fe_{0.33}Cr_{0.03})(Si_{3.63}Al_{0.37})O_{10}(OH)_2 \bullet 4(H_2O)$ as reported by Zolensky, 1997) that retained structural water even after delivery to the lunar surface (Figs. S-4, S-5 and S-6) (Zolensky, 1997). This is consistent with low EPMA analytical totals of 91-93 wt% obtained on matrix areas (Table S-3), since water/OH is not measured by EPMA. Lath shaped sulphides (~5.3% by area; Fig. 3) comprise pyrrhotite, pentlandite, and rare chalcopyrite –

including the large rectangular sulphide crystal in the middle of the sample (Fig. 1). Manganese-rich ilmenite occurs at trace levels (~0.3% by area). Low-temperature aqueous alteration minerals include framboidal and plaquet magnetite (~12.4% by area; Fig. 3). The Bench Crater meteorite also contains Ca-rich minerals including calcite and dolomite (~2.4% by area) and apatite (~2.3% by area). Apatite is typically found within the aqueously altered chondrules, is Cl-poor, and is characterised by low F abundance (0.8-1.1 wt%; Table S-3) compared to apatite in indigenous lunar samples, which typically contains at least 3 wt% F (e.g., McCubbin *et al*., 2015).

5.2. Agglutinitic rim

The meteorite fragment has a patchy thin (<100 μm) vesicular crust (Figs. 1 and 4), coating about 10 % of its exterior. This crust is more feldspathic (12.8 ± 0.2 wt.% Al_2O_3) and enriched in TiO_2 (2.2 ± 0.2 wt% TiO_2) compared to carbonaceous chondrite meteorites (<5 wt% Al_2O_3, <0.3 wt% TiO_2; Nittler *et al.*, 2014), and instead is more similar to Apollo 12 bulk regolith compositions (13.9 ± 2.3 wt% Al_2O_3, 3.1 ± 1.1 wt% TiO_2; Graf, 1993) (Table S-3). As the Moon has no atmosphere, this crust is not a fusion crust (formed on Earth during breakup of bolides as they are frictionally heated during atmospheric entry), but is more akin to agglutinitic or splash coat crusts found on rocks in the lunar regolith formed from flash impact melting. The lunar-like composition of the vesicular rim (Table S-3) suggests interaction between the impactor and melted local basaltic lunar regolith either during or after its delivery. Temperatures of ~1100 °C are required to melt lunar regolith (Colozza, 1991). Therefore, some areas of the outer 10-30 μm of Bench Crater have likely been affected by flash heating, provoking dehydration of the matrix to form fibrous material (Fig. 4). However, the occurrence of hydrated saponite-bearing matrix (Fig. 4) just >50 μm away from

the glassy coat suggests that heat was quickly dissipated, and that the internal part of the sample was not baked and extensively degassed during the agglutination process.

5.3. Oxygen isotopes

To try to classify Bench Crater's parent meteorite group, we measured *in situ* the oxygen isotope composition of magnetite, carbonate and the groundmass of the aqueously altered chondrules (within both intermediate phase and amorphous material). In matrix areas, the $\delta^{18}O$ and $\delta^{17}O$ values range from ~9.9 to 16.8‰ and 5.2 to 8.3‰ (Table 2), respectively, generally falling along the terrestrial fractionation line (TFL), between the O isotope compositions of the matrices of CM and CI carbonaceous chondrite falls (Fig. 5). The magnetite $\delta^{18}O$ and $\delta^{17}O$ values range from ~5.7 to 8.5‰ and 4.8 to 6.1‰ (Table 2), respectively, and fall above the TFL, on the same mass dependent fractionation line than the one defined by O isotope compositions of magnetite in CI and CM carbonaceous chondrite falls (Fig. 5). The two carbonate analyses yielded O isotope compositions roughly similar to those measured in the aqueously altered chondrules, plotting at the ^{16}O-rich end of the trend defined by carbonate analysis in CM chondrite falls (Fig. 5).

5.4. Hydrogen, carbon and nitrogen isotopes

We removed a small portion of the matrix of the Bench Crater meteorite and analysed its H, C and N isotope compositions *in situ* in two different 15 × 15 µm areas (see Fig. 1 for location of sampled material) (Fig. 6, Fig. S-10). These two areas yielded bulk δD values of -36 ± 40 and +200 ± 40 ‰ (all uncertainties on isotopic ratios given at 2σ), $\delta^{13}C$ values of -2 ± 20 and -23 ± 20 ‰, and $\delta^{15}N$ values of -27 ± 20 and -52 ± 20 ‰ (Figs. 7 and 8; Table 1). Two additional 10 × 10 µm areas analysed only for their H isotope compositions yielded bulk δD values of -13 ± 18 and +35 ± 18 ‰. The variability in δD values measured in the four

analysed areas likely relates to variable proportions of H-bearing silicates to insoluble organic matter, since these two hosts of hydrogen in carbonaceous chondrites have generally very different δD values (e.g., Alexander *et al.*, 2007, 2012). Overall, the Bench Crater meteorite is characterised by δD values ranging between -36 ± 40 and 200 ± 40 ‰, and bulk average $\delta^{13}C$ of -13 ± 30 ‰ (2 SD, n = 2) and $\delta^{15}N$ of -40 ± 36 ‰ (2 SD, n = 2) (Table 1).

NanoSIMS imaging did not show any micron-size H-, C- or N-isotopically anomalous regions (Fig. 6 and Figs. S-9 and S-10), contrary to what is observed in interplanetary dust particles (IDPs), ultracarbonaceous Antarctic micrometeorites, and the most primitive chondrites like Murchison, in which hotspots with elevated isotope ratios are common (Figs. S-9 and S-10) (*e.g.*, Messenger, 2000; Nakumura-Messenger *et al.*, 2006; Duprat *et al.*, 2010 ; Remusat et al. 2016). There was also no isotopic distinction between C-rich and C-poor areas of the Bench Crater samples (Fig. 6).

6. Discussion

The Bench Crater meteorite provides the first direct evidence of surviving hydrated carbonaceous chondrite material delivered to the lunar regolith (Zolensky, 1997). It is, thus, currently the only direct ground-truth of the planetary end-member for all H, N and C light-element isotopic analysis of lunar soils. These findings provide important benchmarks for models of volatile processing and transport across the lunar surface (Benna *et al.* 2019).

6.1. Bench Crater meteorite classification

The Bench Crater meteorite is mineralogically and compositionally unusual compared with other carbonaceous chondrite groups. It is mineralogically distinct from CV types, which are lacking in calcite and dolomite and have comparatively lower abundances of phyllosilicates

(1.9–4.2%) and magnetite (6 %) (Howard *et al.*, 2010) than Bench Crater (Figure 3). Affinities have previously been made with C-ungrouped types (McSween, 1976; Fitzgerald and Jones 1977) and CM2 carbonaceous chondrites (Zolensky *et al.*, 1996). For instance, the high abundance of acicular sulphides and the presence of aqueously altered chondrules are similar to the CM1/2 Boriskino meteorite (Vacher *et al.*, 2018; Verdier-Paoletti *et al.*, 2019) and thermally metamorphosed CI, CM and CY chondrites (e.g., Ikeda, 1992; Tonui *et al.*, 2014; King *et al.*, 2019a). However, the high modal abundance of magnetite bears more resemblance to CI chondrites and matrix-rich (altered) CR chondrites such as Al Rais and Grove Mountains (GRO) 95577 (Fig. 3). Notably the meteorite matrix is magnesian and is compositionally more similar to CI-meteorite groups than CM or CR types (Fig. S-6) (van Kooten *et al.*, 2018), suggesting a higher state of parent body aqueous alteration. It should be noted that minor dehydration due thermal processing is unlikely to have changed the MgO/FeO ratio; this ratio being constant in CM chondrites having experienced dehydration (Lipschutz *et al*., 1999). Bench Crater also share similarities with the Lonewolf Nunataks (LON) 94101 meteorite, which has been described as a CM chondrite with coarse acicular sulphides and a wide variety of CM- and magnetite-rich CI-like clasts (Lindgren *et al*., 2013). Bench Crater might be akin a clast-rich CM chondrite, but its limited size and hence representativeness precludes definitive assessment of this possibility. All these observations indicate that the Bench Crater meteorite cannot be directly related to any known carbonaceous chondrite groups present in our current meteorite collections.

Bench Crater meteorite also shows oxygen isotope characteristics that connect it to the hydrated CI and CM carbonaceous chondrites. For example, the Bench Crater magnetite grains have O isotope compositions that are on the same mass fractionation line as magnetite in CI and CM chondrite groups (Fig. 5). Furthermore, Bench Crater carbonates are

characterised by O isotope compositions plotting at the ^{16}O-rich end of the trend defined by carbonates from CM2 chondrite falls (Fig. 5) (Verdier-Paoletti *et al.*, 2017; Vacher *et al.*, 2018) and some CM1 chondrites from the Antarctic meteorite collection (Allan Hills 83100, Allan Hills 84034 and Meteorite Hills 01070; Telus *et al.*, 2019). The O isotope composition of silicates in Bench Crater aqueously altered chondrules plots along the TFL, similarly to the O isotope compositions measured in bulk CI chondrites and in their matrix and most olivine grains (Fig. 5) (e.g., Leshin *et al.*, 1997; Piralla *et al.*, 2020). The O isotope compositions of silicates in aqueously altered chondrules yield an average Δ^{17}O of -0.12 ± 0.45 ‰. Such a Δ^{17}O value is, within errors, intermediate between the Δ^{17}O of CI chondrite matrix (0.37 ± 0.42 %) and to that of CM chondrite matrix (Δ^{17}O = -1.76 ± 0.63 ‰) (e.g., Clayton and Mayeda, 1984, 1999). Finally, the δ^{17}O and δ^{18}O isotope ratios in Bench Crater component are significantly lower than $\delta^{17,18}$O values of bulk CY chondrites (Tonui *et al.*, 2014; King *et al.*, 2019a).

The evolution of the Δ^{17}O values in Bench Crater meteorite components implies that the oxygen isotope compositions of secondary phases (magnetite, carbonates) did not result from fluid circulation along a temperature gradient, which would produce a trend with a slope of 0.52. Instead, variations of Δ^{17}O values imply that the main process controlling the O isotope compositions of the Bench Crater secondary phases is related to isotopic equilibrium between ^{16}O-rich anhydrous silicates and ^{17}O- and ^{18}O-rich fluids as commonly reported in CM chondrites (e.g., Verdier-Paoletti *et al.*, 2017; Marrocchi *et al.*, 2018). In this scenario, magnetite would correspond to early precipitates whereas carbonates formed after significant hydrothermal alteration. Furthermore, the carbonate O isotope compositions show similarity with those reported in CM chondrites whose precipitation temperatures were estimated to be < 200°C (Vacher *et al.*, 2019a). This suggests that Bench Crater did not experience

significant heating and dehydration processes, although the lack of tochilinite would suggest a temperature higher than 320°C (Pignatelli *et al.*, 2017). However, we note that the stability field of tochilinite is strongly affected by Mg-Fe substitutions (Kozerenko *et al.*, 1996, 2001) and is not well constrained (Vacher *et al.*, 2019b).

Taken together, the oxygen isotope composition of Bench Crater mineral phases (Fig. 5), along with its modal mineralogy (Fig. 3) and matrix composition (Fig. S-6), do not exactly match that of a known carbonaceous chondrite group. It might represent a rare type of carbonaceous asteroid parent body that is currently unsampled in the Earth's meteorite collection. However, Bench Crater has important similarities with carbon-rich hydrated CI and CM chondrites; the differences could be related to greater amounts of water ice grains originally accreted by the Bench Crater parent body. Such a hypothesis could be tested thanks to several assumptions, and following the methodology applied to CM, CO, CR and CV carbonaceous chondrites (Marrocchi *et al.*, 2018). Bench Crater carbonates show $\delta^{17,18}O$ values plotting on the CM Ca-carbonate trend (Vacher *et al.*, 2016, 2018; Verdier-Paoletti *et al.*, 2017), suggesting they precipitated from water with a similar O isotope evolution than that of CM chondrites. Assuming that the bulk oxygen isotope composition of Bench Crater is similar to the most altered CM chondrites (i.e., $\delta^{18}O$ = 10 ‰; Clayton and Mayeda, 1984, 1999) and considering the O isotope composition of anhydrous CM silicates as plausible Bench Crater protolith (i.e., $\delta^{18}O$ = -4.2 ‰; Clayton and Mayeda, 1984, 1999), we calculated the water/rock ratio at different temperature ranging from 25 to 150°C. This gives a water/rock ratio for Bench Crater in the range 0.35 to 0.55, which is slightly higher than for most CM chondrites that are characterised by a narrow range of water/rock ratio of 0.3-0.4 irrespective of their petrological type (e.g., Zolensky *et al.*, 1997; Marrocchi *et al.*, 2018). Although speculative, these results suggest than the Bench Crater asteroidal parent-body was

more water-rich than the source location(s) of other CM chondrites. In addition, the physio-chemical conditions of hydrothermal alteration in the Bench Crater parent-body (e.g., Palguta et al., 2010; Travis and Schubert, 2005) might have been different than in other CM chondrite original parent body(ies), as indicated by the higher abundance of magnetite in Bench Crater compared to most CM chondrites (i.e., 12.4 % by area vs. 1.1-2.4 vol.%, see Fig. 3), and the lack of tochilinite.

6.2. Thermal and shock history of the Bench Crater meteorite

The agglutinitic rim of Bench Crater indicates that it has been affected by flash heating on the lunar surface, but that such effects only affected the outer ~10-30 µm of the fragment. Matrix mineralogy and chemical composition also allows assessing the thermal history of the Bench Crater fragment as a whole. Low analytical totals obtained through EPMA analyses in the matrix of Bench Crater (91-93 wt%; Table S-3) may be related to the presence of microporosity, and/or species not accounted for during EPMA analysis such as water/OH and/or carbon. TEM observation of saponite in the matrix suggests that the missing 7-9 wt% are likely related to the presence of water and/or OH. However, low EPMA totals obtained in Bench Crater matrix are higher than those typically recorded in unmodified CI and CM meteorite matrix (Lee *et al.* 2016), and more similar to carbonaceous chondrite types that have undergone a small degree of dehydration from thermal processing at around 500-600°C (Nakamura 2006, Lee *et al.*, 2016).

Peak temperatures experienced by the bulk Bench Crater meteorite can be constrained by petrographic observations. The preservation of saponite indicates that the bulk meteorite did not experience heating over ~700-900°C, as saponite has been shown to fully decompose above these temperatures (e.g., Akai, 1997; Nozaki et al., 2006). Moreover, temperatures

cannot have exceeded *ca*. 600-700 °C as carbonates are not decomposed and no vesicles can be seen in calcite phases (from CO_2 loss) (Fig. S-8), (e.g, Nakamura, 2006; Nozaki *et al.*, 2006). As no serpentine is observed in the Bench Crater sample matrix, heating may have occurred at temperatures between ~400 and 800°C as serpentine breaks down by ~400°C (Tomioka *et al.,* 2007). Boundaries of the aqueously altered chondrules are generally well preserved (Figs. 1 and 2), analogous to those observed in carbonaceous chondrite heating experiments <600 °C (Tonui *et al.,* 2014). Interestingly, ca. 600 °C also corresponds to the temperature where hydrogen isotope anomaly hotspots have been shown to disappear in Murchison organics (Remusat *et al.,* 2016), which may account for the absence of hydrogen hotspots in Bench Crater. Therefore, we estimate that the bulk Bench Crater meteorite underwent heating between ~400-600 °C, which was enough to partially, but not totally, dehydrate the fine-grained matrix.

It is challenging to determine if heating of Bench Crater was caused by asteroidal parent body processes (for example, internal heating from ^{26}Al decay, impact metamorphism, flash heating from solar irradiation during an orbital transfer close to the Sun; Nakamura 2006; Nakato *et al.,* 2008), during the impact event that delivered Bench Crater to the Moon, or during lunar surface residence (*e.g.*, repeated diurnal thermal cycling, flash heating from other impact events). It is generally thought that thermal metamorphism that has affected the dozens of heated CM chondrites was short lived and took place billions of years after the formation of the Solar System, ruling out internal heating from ^{26}Al decay as a possible cause (e.g., King *et al.*, 2019b; Amsellem *et al.*, 2020). If heating of Bench Crater took place on its parent body the remaining options then include short-lived impact-related metamorphism or solar irradiation. The Bench Crater meteorite does not have a strong petrofabric (Fig. 1), unlike some of the shocked CM chondrite types studied by Lindgren *et al.* (2015) and Vacher

et al. (2018), suggesting that it has not been highly shocked. However, intermediate phase (i.e., decomposed phyllosilicates) similar to that observed in Bench Crater was observed during <21-30 GPa peak pressure impact experiments on the Murchison (CM2) meteorite (Tomioka *et al.*, 2007). Thus, it is difficult to further discriminate whether shock metamorphism or solar irradiation were responsible for heating of Bench Crater if metamorphism took place on its parent body.

6.3. Isotopic fractionation effects

Hydrogen in carbonaceous chondrites is hosted within both phyllosilicate and organic phases, whereas carbon and nitrogen are mostly hosted within organic components, and to a lesser extent within carbonates for carbon (e.g., Pearson *et al.*, 2006; Alexander et al., 2007, 2012; Füri and Marty, 2015; van Kooten *et al.*, 2017; Piani and Marrocchi, 2018; Piani *et al.*, 2018). The H and C isotope compositions obtained on two areas of Bench Crater are similar to those obtained on bulk CI and CM chondrite meteorites (Fig. 7). The H isotope compositions measured in Bench Crater is also consistent with the H isotope compositions measured in CI- and CM-like clasts found in Howardite-Eucrite-Diogenite meteorites (Patzek *et al.*, 2020). On the other hand, the N isotope composition of Bench Crater is intermediate between the bulk $\delta^{15}N$ values of CI-CM chondrites and the bulk $\delta^{15}N$ value of the 12037 soil (Figs. 7 and 8, Table S-2). Figure 7 indicates that there may be some slight δD, $\delta^{13}C$ and $\delta^{15}N$ variability between the two area analysed that may relate to sample heterogeneity on the scale of a few microns. Alternatively, the observed δD, $\delta^{13}C$ and $\delta^{15}N$ variations may be related to localised impact shock-induced volatile element isotopic fractionation (Tomioka *et al.*, 2007). It is easier to 'lose' the isotopes ^{13}C, ^{15}N and H mostly bound in inorganic phyllosilicate components in CI-CM type chondrites than ^{12}C, ^{14}N and D that are mostly bound in insoluble organic matter, as has been shown for CM chondrites during 30-40 GPa peak shock pressure

impact events (*i.e.* <1.5 km/s velocities) (Tyburczy *et al.*, 2001). Starting from CM chondrite-like H, C and N isotope characteristics, such a process could qualitatively explain the concomitant δD increase and $\delta^{13}C$-$\delta^{15}N$ decrease observed for the two areas analysed in the Bench Crater meteorite.

6.4. Implications for the survivability of hydrated asteroids and their volatile budgets delivered to the lunar surface

Nitrogen isotopes: The wide range of isotope signatures observed for N trapped in the lunar regolith is consistent with varying mixing proportions between isotopically light solar wind N ($\delta^{15}N$ around -400 ‰) and a more ^{15}N-rich 'planetary' component (Hashizume et al., 2000; Füri and Marty, 2015; Füri *et al.*, 2015; Mortimer *et al.*, 2016) (Fig. 8). The Bench Crater $\delta^{15}N$ value of -40 ± 18 ‰ is lower than bulk N isotope compositions of CI-CM carbonaceous chondrite meteorites (Fig. 7). This may indicate that Bench Crater sampled an asteroidal parent-body not represented in the meteorite collection. However, the original N isotope composition of Bench Crater may have also been modified on the lunar surface. Its $\delta^{15}N$ value is intermediate between that of the bulk 12037 soil and bulk CI-CM chondrite $\delta^{15}N$ values (Fig. 7), which may indicate that the original N isotope composition of Bench Crater has been lowered due to isotopic exchange with N in the target mare basaltic Apollo 12 soil, possibly during the flash-heating event that formed the meteorite's agglutinitic rim (Fig. 4). However, this latter scenario seems unlikely since CM-like chondrites contain more than one order of magnitude more N (~600 to 1000 ppm; Pearson *et al.*, 2006; Alexander *et al.*, 2012) compared to the 12037 bulk soil (~40 ppm; Becker and Clayton, 1978; Kerridge *et al.*, 1978).

Hydrogen isotopes: In situ analyses of Apollo soil and agglutinate particles have yielded a large range of D/H ratios, suggesting mixing between nearly D-free implanted solar wind (δD

~ -1000 ‰) and H-bearing sources with higher D/H ratios that may include reworked (melted) material from vaporisation of impacting D-rich organics or water-bearing asteroids, interplanetary dust particles (IDPs) and comets, volcanic gases, or caused by a spallogenic component (Liu *et al.*, 2012; Stephant and Robert, 2014). Bench Crater has δD values ranging between -36 ± 40 and 200 ± 40 ‰ (Figs. 7 and 8). It is unlikely that the D/H ratio of Bench Crater hydrogen-bearing species could have been significantly altered by interacting with low D/H hydrogen derived from the lunar target soil since CM-like chondrites contain more than two orders of magnitude more H (*ca*. 1-1.5 wt%; e.g., Alexander *et al.*, 2012) than Apollo 12 bulk soils (*ca*. 10-100 ppm; e.g., Carter, 1985). Instead we interpret that this range of δD values of 0-200 ‰ likely corresponds to the bulk original H isotope composition of the Bench Crater parent body, which is consistent with bulk H isotope compositions measured in CI and CM chondrites (Figs. 7 and 8).

7. Conclusions

The survivability of hydrated asteroidal material in Apollo 12 soil 12037 indicates that (i) delivered volatiles are stable against small meteoritic impact events at the Moon's surface, and (ii) agglutination of impactor particles either during the impact event, or subsequently during lunar regolith gardening, does not necessarily cause complete degassing and dehydration or light stable isotope fractionation of delivered hydrated material. These findings provide important constraints to ground-truth future lunar prospecting missions that will investigate the volatile concentration and isotopic composition of the lunar regolith at, and below, the surface (e.g., Carpenter *et al.*, 2014; Colaprete *et al.*, 2016; Barber *et al.*, 2017). Bench Crater provides critical constraints for these exploration activities that aim to identify the sources of different volatile species with depth and time.

Bench Crater bears some resemblance with highly aqueously altered and/or brecciated CM chondrites such as Boriskino (Vacher *et al.,* 2018; Verdier-Paoletti *et al.,* 2019) and LON 94101 (Lindgren *et al*., 2013). However, fully evaluating the possibility that Bench Crater is a CI-like clast-rich brecciated CM chondrite is hindered by its limited size and thus representativeness. With this caveat in mind, detailed mineralogical, geochemical, and isotopic data obtained on Bench Crater might also suggest that it is unique compared with known carbonaceous meteorite groups present in our meteorite collection, providing evidence for delivery of a sample from a previously unknown type of mildly thermally processed carbonaceous asteroid parent body. Other types of potentially unique partially thermally heated carbonaceous chondrite clasts have also been observed in other planetary regolith samples, including those from the howardite and ureilite parent bodies (Zolensky *et al.*, 2019 and references therein). These thermally processed carbonaceous meteorites can provide important constraints for interpreting spectral observations of the surface of carbonaceous asteroids that likely host a mixture of hydrated and dehydrated phases (e.g., King *et al.*, 2019). In addition, they may provide a close match to samples that will be brought back from asteroid 162173 Ryugu by the Hayabusa2 spacecraft in 2020, since spectral characteristics of its surface are consistent with those of thermally metamorphosed CI-CM-CY carbonaceous chondrites (*e.g.*, King *et al.*, 2019a; Kitazato *et al.*, 2019).

Altogether, Bench Crater mineralogical, geochemical and isotopic characteristics do not match any other types of carbonaceous chondrite present in our collections. Given that Bench Crater may have been delivered to the Moon anytime in the last 100 Myr, this may indicate a recent change in sources of materials impacting the Earth-Moon system. Identifying such changes would help to better understand the sources and causes of impact bombardment, providing better constraints to refine theoretical Solar System models (*e.g.,* Wetherill, 1975)

474 and track the migration of volatile-rich planetary bodies into the inner Solar System through
475 time (Joy *et al.*, 2016).
476
477
478 **References**
479
480 Akai, J., 1997. T-T-T diagram of serpentine and saponite, and estimation of metamorphic
481 heating degree of Antarctic carbonaceous chondrites Sixteenth Symposium on Antarctic
482 Meteorites. Proceedings of the NIPR Symposium, No. 5. p.120.
483 Alexander, C.M.O'D., Bowden, R., Fogel, M.L., Howard, K.T., Herd, C.D.K., Nittler, L.R.,
484 2012. The provenances of asteroids, and their contributions to the volatile inventories of
485 the terrestrial planets. Science 337, 721-723.
486 Alexander, C.M.O'D., Fogel, M., Yabuta, H., Cody, G.D., 2007. The origin and evolution of
487 chondrites recorded in the elemental and isotopic compositions of their macromolecular
488 organic matter. Geochimica et Cosmochimica Acta 71, 4380-4403.
489 Amsellem, E., Moynier, F., Mahan, B., Beck, P., 2020. Timing of thermal metamorphism in
490 CM chondrites: Implications for Ryugu and Bennu future sample return. Icarus 339,
491 113593.Anand, M., Crawford, I.A., Balat-Pichelin, M., Abanades,S., van Westrenen, W.,
492 Péraudeau, G., Jaumann R., Seboldt, W., 2012. A brief review of chemical and
493 mineralogical resources on the Moon and likely initial in situ resource utilization (ISRU)
494 applications. Planetary and Space Science 74, 42-48.
495 Arvidson, R., Crozaz, G., Drozd, R. J., Hohenberg, C. M., Morgan, C. J., 1975. Cosmic ray
496 exposure ages of features and events at the Apollo landing sites. The Moon 13, 259-276.
497 Avdellidou, C., Price, M. C., Delbo, M., Ioannidis, P., Cole, M. J., 2016. Survival of the
498 impactor during hypervelocity collisions – I. An analogue for low porosity targets

499 Monthly Notices of the Royal Astronomical Society 456, 2957-2965.
500 doi: 10.1093/mnras/stv2844.
501 Barber, S.J., Smith, P.H., Wright, I.P., Abernethy, F., Anand, M., Dewar, K.R., Hodges, M.,
502 Landsberg, P., Leese, M.R., Morgan, G.H., Morse, A.D., 2017. ProSPA: the science
503 laboratory for the processing and analysis of lunar polar volatiles within PROSPECT. 48th
504 Lunar and Planetary Science Conference, 20-24 Mar 2017, The Woodlands, Houston,
505 Texas. Abstract 2171.
506 Becker, R. H., Clayton, R. N., 1978. Nitrogen isotope systematics of two Apollo 12 soils. In:
507 Lunar and Planetary Science Conference, 9th, Houston, Tex., March 13-17, 1978,
508 Proceedings. Volume 2. (A79-39176 16-91) New York, Pergamon Press, Inc., 1978, p.
509 1619-1627.
510 Benna, M., Hurley, D.M., Stubbs, T.J., Mahaffy, P.R., Elphic, R.C., 2019. Lunar soil
511 hydration constrained by exospheric water liberated by meteoroid impacts. Nature
512 Geoscience 12, 333-338 doi.org/10.1038/s41561-019-0345-3
513 Burnett, D. S., Drozd, R. J., Morgan, C. J., Podosek, F. A., 1975. Exposure histories of Bench
514 Crater rocks. In: Lunar Science Conference, 6th, Houston, Tex., March 17-21, 1975,
515 Proceedings. Volume 2. (A78-46668 21-91) New York, Pergamon Press, Inc., 1975, p.
516 2219-2240.
517 Carpenter, J. D., Barber, S., Cerroni, P., Fisackerly, R., Fumagalli, A., Houdou, B., Howe, C.,
518 Magnani, P. G., Morse, A., Monchieri, E., Reiss, P., Richter, L., Rizzi, F., Sheridan, S.,
519 Waugh, L., Wright, I. P., 2014. Accessing and assessing lunar resources with PROSPECT.
520 In: Annual Meeting of the Lunar Exploration Analysis Group, 22-24 October, 2014 ,
521 Laurel, Maryland, USA.
522 Cockell, C. S., 2010. Astrobiology-What Can We Do on the Moon? Earth, Moon and
523 Planets 107, 310.

Colozza, A. J., 1991. Analysis of lunar regolith thermal storage energy International Solar Energy Conference; Lahaina, HI; United States. Report: NASA-CR-189073

Colaprete, A., Elphic, R.C., Andrews, D., Bluethmann, W., Quinn, J., Chavers, D.G., 2016. Resource Prospector: Evaluating the ISRU Potential of the Lunar Poles. Presentation to the Lunar Exploration Analysis Group (LEAG). Nov 2 2016.

Barnes, J. J., Kring, D. A., Tartèse, R., Franchi, I. A., Anand, M., Russell, S.S., 2016. An asteroidal origin for water in the Moon. Nature Communications 7, doi:10.1038/ncomms11684.

Carter, J.L., 1985. Lunar regolith fines-A source of hydrogen. In Lunar bases and space activities of the 21st century. pp. 571-581.

Clayton, R. N., Mayeda, T. K., 1984. The oxygen isotope record in Murchison and other carbonaceous chondrites. Earth Planetary Science Letters 67, 151-161.

Clayton, R. N., Mayeda T. K., 1999. Oxygen isotope studies of carbonaceous chondrites. Geochimica et Cosmochimica Acta 63, 2089-2104.

Curran N., Nottingham, M., Alexander, L., Crawford, I. A., Füri, E., Joy, K. H., 2020. Database of Noble Gases in Lunar Samples in Preparation for Mass Spectrometry on the Moon. Planetary and Space Science 182, 104823. doi.org/10.1016/j.pss.2019.104823

Davy, R., Whitehead, S. G., Pitt, G., 1978. The Adelaide Meteorite. Meteoritics, 13(1), 121-140. doi:10.1111/j.1945-5100.1978.tb00802.x

Duprat, J., Dobrică, E., Engrand, C., Aléon, J., Marrocchi, Y., Mostefaoui, S., Meibom, A., Leroux, H., Rouzaud, J.N., Gounelle, M., Robert, F., 2010. Extreme deuterium excesses in ultracarbonaceous micrometeorites from central Antarctic snow. Science 328(5979), 742-745.

Fitzgerald, M. J., Jones, J. B., 1977. Adelaide and Bench Crater - Members of a new subgroup of the carbonaceous chondrites. Meteoritics 12, 443-458.

549 Füri E., Marty, B., 2015. Nitrogen isotope variations in the Solar System. Nature Geoscience 8,
550 515–522. doi:10.1038/ngeo2451.
551 Füri, E., Marty, B., Assonov, S. S., 2012. Constraints on the flux of meteoritic and cometary
552 water on the Moon from volatile element (N-Ar) analyses of single lunar soil grains, Luna
553 24 core. Icarus 218, 220-229.
554 Füri, E., Deloule, E. and Trappitsch, R., 2017. The production rate of cosmogenic deuterium
555 at the Moon's surface. Earth and Planetary Science Letters, 474, 76-82.
556 Füri, E., Zimmermann, L., Saal, A.E., 2018. Apollo 15 green glass He-Ne-Ar signatures–In
557 search for indigenous lunar noble gases. Geochemical Perspectives Letters, 8, 1-5.
558 Flynn, G. J., Consolmagno, G. J., Brown, P., Macke, R. J., 2017. Physical properties of the
559 stone meteorites: Implications for the properties of their parent bodies. Chemie der Erde
560 3, 269-298.
561 Graf, J.C., 1993. Lunar Soils Grain Size Catalog NASA Reference Publication 1265
562 Hashizume, K., Chaussidon, M., Marty, B., Robert, F., 2000. Solar Wind Record on the
563 Moon: Deciphering Presolar from Planetary Nitrogen. Science 290, 1142-1145.
564 Heck, P. R., Schmitz, B., Bottke, W. F., Rout, S. S., Kita, N. T., Cronholm, A., Defouilloy,
565 C., Dronov, A., Terfelt, F., 2017. Rare meteorites common in the Ordovician
566 period. Nature Astronomy 1, doi:10.1038/s41550-016-0035.
567 Howard, K.T., Benedix, G.K., Bland, P.A., Cressey, G., 2010. Modal mineralogy of CV3
568 chondrites by X-ray diffraction (PSD-XRD). Geochimica et Cosmochimica Acta 74(17),
569 5084-5097.
570 Howard, K. T., Benedix, G. K., Bland, P. A., Cressey G., 2011. Modal mineralogy of CM
571 chondrites by X-ray diffraction (PSD-XRD). Part 2: Degree, nature and settings of
572 aqueous alteration. Geochimica et Cosmochimica Acta 75, 2735-2751.

573 Howard K. T., Alexander C. M. O'D., Schrader D. L., Dyl K. A., 2015. Classification of
574 hydrous meteorites (CR, CM and C2 ungrouped) by phyllosilicate fraction: PSD-XRD
575 modal mineralogy and planetesimal environments. Geochimica et Cosmochimica Acta
576 149, 206-222.
577 Ikeda, Y., 1992. An overview of the research consortium, Antarctic carbonaceous chondrites
578 with CI affinities, Yamato-86720, Yamato-82162, and Belgica-7904. Proceedings of the
579 NIPR Symposium on Antarctic Meteorites 5, 49-73.
580 Joy, K. H., Crawford, I. A., Curran, N. A., Zolensky, M. E., Fagan, A. L., Kring, D. A., 2016.
581 The Moon as an Archive of Small Body Migration in the Solar System. Earth, Moon and
582 Planets. doi: 10.1007/s11038-016-9495-0.
583 Joy, K. H., Zolensky, M. E., Nagashima, K., Huss, G. R., McKay, D. S., Ross, D. K., Kring,
584 D. A., 2012. Direct detection of projectile relics from the end of the lunar basin-forming
585 epoch. Science 336, 1426-1429. doi 10.1126/science.1219633.
586 Kozerenko S.V., Fadeev V.V., Organova N.I., Chstyakova N.I., Kolpakova N.N., Senin V.G.,
587 2001. Synthesis, formation conditions and crystallochemistry of tochilinites – iron,
588 magnesium and sodium hydroxide-sulfides. Experiment in Geosciences 10, 57-58.
589 Kozerenko, S.V., Organova, N.J., Fadeev, V.V., Magazina, L.O., Kolpakova, N.N. and
590 Kopneva, L.A., 1996. Tochilinite Produced in Laboratory. Lunar and Planetary Science
591 Conference, XXVII, 695-696.
592 Kerridge, J.F., Kaplan, I.R., Kung, C.C., Winter, D.A., Friedman, D.L., DesMarais, D.J.,
593 1978. Light element geochemistry of the Apollo 12 site. Geochimica et Cosmochimica
594 Acta 42, 391-402.
595 King, A. J., Schofield P. F., Howard K. T., Russell S. S., 2015. Modal mineralogy of CI and
596 CI-like chondrites by X-ray diffraction. Geochimica et Cosmochimica Acta 165, 148-160.

King, A. J., Schofield P. F., Russell, S. S., 2017. Type 1 aqueous alteration in CM carbonaceous chondrites: Implications for the evolution of water-rich asteroids. Meteoritics & Planetary Science 52, 1197-1215.

King, A.J., Bates, H.C., Krietsch, D., Busemann, H., Clay, P.L., Schofield, P.F., Russell, S.S., 2019a. The Yamato-type (CY) carbonaceous chondrite group: Analogues for the surface of asteroid Ryugu? Geochemistry 79, 125531.

King, A.J., Russell, S.S., Schofield, P.F., Humphreys-Williams, E.R., Strekopytov, S., Abernethy, F.A.J., Verchovsky, A.B., Grady, M.M., 2019b. The alteration history of the Jbilet Winselwan CM carbonaceous chondrite: An analog for C-type asteroid sample return. Meteoritics & Planetary Science 54, 521-543.

Kitazato, K., Milliken, R.E., Iwata, T., Abe, M., Ohtake, M., Matsuura, S., Arai, T., Nakauchi, Y., Nakamura, T., Matsuoka, M., Senshu, H., Hirata, N., Hiroi, T., Pilorget, C., Brunetto, R., Poulet, F., Riu, L., Bibring, J.-P., Takir, D., Domingue, D.L., Vilas, F., Barucci, M.A., Perna, D., Palomba, E., Galiano, A., Tsumura, K., Osawa, T., Komatsu, M., Nakato, A., Arai, T., Takato, N., Matsunaga, T., Takagi, Y., Matsumoto, K., Kouyama, T., Yokota, Y., Tatsumi, E., Sakatani, N., Yamamoto, Y., Okada, T., Sugita, S., Honda, R., Morota, T., Kameda, S., Sawada, H., Honda, C., Yamada, M., Suzuki, H., Yoshioka, K., Hayakawa, M., Ogawa, K., Cho, Y., Shirai, K., Shimaki, Y., Hirata, N., Yamaguchi, A., Ogawa, N., Terui, F., Yamaguchi, T., Takei, Y., Saiki, T., Nakazawa, S., Tanaka, S., Yoshikawa, M., Watanabe, S., Tsuda, Y., 2019. The surface composition of asteroid 162173 Ryugu from Hayabusa2 near-infrared spectroscopy. Science 364, 272-275.

Lee, M.R., Lindgren, P., King, A.J., Greenwood, R.C., Franchi, I.A. and Sparkes, R., 2016. Elephant Moraine 96029, a very mildly aqueously altered and heated CM carbonaceous

621 chondrite: Implications for the drivers of parent body processing. Geochimica et
622 Cosmochimica Acta 187, 237-259.
623 Leshin, L.A., Rubin, A.E., McKeegan, K.D., 1997. The oxygen isotopic composition of
624 olivine and pyroxene from CI chondrites. Geochimica et Cosmochimica Acta 61, 835-845.
625 Li S., Lucey, P. G., Milliken, R. E., Hayne, P. O., Fisher, E., Williams, J.-P., Hurley, D.
626 M., Elphic, R. C. 2018. Direct evidence of surface exposed water ice in the lunar polar
627 regions. Proceedsings of the National Academy of Sciences 115 (36), 8907-8912.
628 Lindgren, P., Lee, M.R., Sofe, M.R. and Zolensky, M.E., 2013 Clasts in the CM2
629 carbonaceous chondrite Lonewolf Nunataks 94101: Evidence for aqueous alteration prior
630 to complex mixing. Meteoritics & Planetary Science 48, 1074-1090.
631 Lindgren, P., Hanna, R. D., Dobson, K. J., Tomkinson, T., Lee, M. R., 2015. The paradox
632 between low shock-stage and evidence for compaction in CM carbonaceous chondrites
633 explained by multiple low-intensity impacts. Geochimica et Cosmochimica Acta 148, 159-
634 178.
635 Lipschutz M.E., Zolensky M.E., Sue M. 1999. New petrographic and trace element data on
636 thermally metamorphosed carbonaceous chondrites. Antarct. Meteorite Res. 12, 57-80
637 Liu, Y., Guan, Y., Zhang, Y., Rossman, G. R., Eiler, J. M., Taylor, L. A., 2012. Direct
638 measurement of hydroxyl in the lunar regolith and the origin of lunar surface water.
639 Nature Geoscience 5, 779-782. doi:10.1038/NGEO1601.
640 Marrocchi, Y., Bekaert, D.V., Piani, L., 2018. Origin and abundance of water in
641 carbonaceous asteroids. Earth and Planetary Science Letters 482, 23-32.
642 Martins Z., Price, M. C., Goldman, N., Sephton, M. A., Burchell, M. J., 2013. Shock synthesis
643 of amino acids from impacting cometary and icy planet surface analogues. Nature Geoscience 6,
644 1045-1049. doi:10.1038/ngeo1930.

McCubbin, F. M., Vander Kaaden, K. E., Tartèse, R., Klima, R. L., Liu, Y., Mortimer, J., Barnes, J. J., Shearer, C. K., Treiman, A. H., Lawrence, D. J., Elardo, S. M., Hurley, D. M., Boyce, J. W., Anand, M., 2015. Magmatic volatiles (H, C, N, F, S, Cl) in the lunar mantle, crust, and regolith: Abundances, distributions, processes, and reservoirs. American Mineralogist 100, 1668-1707. doi:10.2138/am-2015-4934.

McSween, H. Y. Jr. 1976. A new type of chondritic meteorite found in lunar soil. Earth and Planetary Science Letters 31, 193-199.

Messenger, S., 2000. Identification of molecular-cloud material in interplanetary dust particles. Nature 404, 968-971. doi:10.1038/35010053.

The Meteoritical Bulletin http://www.lpi.usra.edu/meteor/

Nakato, A., Nakamura, T., Kitajima, F., Noguchi, T., 2008. Evaluation of dehydration mechanism during heating of hydrous asteroids based on mineralogical and chemical analysis of naturally and experimentally heated CM chondrites. Earth, Planets and Space, 60(8), 855-864.

Nakamura, T., 2006. Yamato 793321 CM chondrite: Dehydrated regolith material of a hydrous asteroid. Earth and Planetary Science Letters, 242(1-2), pp.26-38.

Nakumura-Messenger, K., Messenger, S., Keller, L. P., Clemett, S. J., Zolensky, M. E., 2006. Organic Globules in the Tagish Lake Meteorite: Remnants of the Protosolar Disk. Science 314, 1439-1442. doi:10.1126/science.1132175.

Nittler, L.R., McCoy, T.J., Clark, P.E., Murphy, M.E., Trombka, J.I., Jarosewich, E., 2004. Bulk element compositions of meteorites: A guide for interpreting remote-sensing geochemical measurements of planets and asteroids. Antarctic Meteorite Research.

Nozaki, W., Nakamura, T., Noguchi, T., 2006. Bulk mineralogical changes during heating in the upper atmosphere at temperatures below 1000°C. Meteoritics & Planetary Science 41, 1095-1114.

NRC (National Research Council), 2007. Report on the Scientific Context for the Exploration of the Moon. Committee on the Scientific Context for Exploration of the Moon Space Studies Board Division on Engineering and Physical Sciences. The National Academies Press, Washington. ISBN: 0-309-10920-5, p. 120.

Palguta, J., Schubert, G., Travis, B.J., 2010. Fluid flow and chemical alteration in carbonaceous chondrite parent bodies. Earth and Planetary Science Letters, 296(3-4), 235-243.

Patzek M., Hoppe P., Bischoff A., Visser, R., John, T., 2020. Hydrogen isotopic composition of CI- and CM-like clasts from meteorite breccias - sampling unknown sources of carbonaceous chondrite materials. Geochimica et Cosmochimica Acta, 272, 177-197 doi.org/10.1016/j.gca.2019.12.017

Pearson, V.K., Septhon, M.A., Franchi, I.A., Gibson, J.M., Gilmour, I., 2006. Carbon and nitrogen in carbonaceous chondrites: Elemental abundances and stable isotopic compositions. Meteoritics & Planetary Science, 41, 1899-1918.

Piani, L., Yurimoto, H., Remusat, L., 2018. A dual origin for water in carbonaceous asteroids revealed by CM chondrites. Nat. Astron. doi:10.1038/s41550-018-0413-4.

Piani L., Marrocchi Y. 2018. Hydrogen isotopic composition of water in CV-type carbonaceous chondrites. *Earth and Planetary Science Letters 504*, 64-71,

Pignatelli I., Marrocchi Y., Mugnaioli E., Bourdelle F., Gounelle M. 2017. Mineralogical, crystallographic and redox features of the earliest stages of fluid alteration in CM chondrites. *Geochimica et Cosmochimica Acta 209*, 106-122.

Piralla, M., Marrocchi, Y., Verdier-Paoletti, M.J., Vacher, L.G., Villeneuve, J., Piani, L., Bekaert, D.V., Gounelle, M., 2020. Primordial water and dust of the Solar System: Insights from in situ oxygen measurements of CI chondrites. Geochimica et Cosmochimica Acta 269, 451-464.

695 Remusat, L., Piani, L., Bernard, S. 2016. Thermal recalcitrance of the organic D-rich
696 component of ordinary chondrites. Earth and Planetary Science Letters 435, 36-44.
697 Rowe, M.W., Clayton, R.N., Mayeda, T. K., 1994. Oxygen isotopes in separated components
698 of CI and CM meteorites. Geochimica et Cosmochimica Acta 58, 5341-5347.
699 Steele A., McCubbin F. M., Fries M., Glamoclija M., Kater L., Nekvasil H., 2010. Graphite
700 in an Apollo 17 Impact Melt Breccia. Science 329, 51. doi:10.1126/science.1190541.
701 Stephant A., Robert F., 2014. The negligible chondritic contribution in the lunar soils water.
702 PNAS 111(42), 15007-15012. doi:10.1073/pnas.1408118111.
703 Syal B., M., Schultz, P. H., 2015. Cometary impact effects at the Moon: Implications for
704 lunar swirl formation. Icarus 257, 194-206. Doi.10.1016/j.icarus.2015.05.005.
705 Svetsov, V.V., Shuvalov, V.V., 2015. Water delivery to the Moon by asteroidal and cometary
706 impacts. Planetary and Space Science, 117,444-452.
707 Telus, M., Alexander, C.M.O'D., Hauri, E.H., Wang, J., 2019. Calcite and dolomite
708 formation in the CM parent body: Insight from *in situ* C and O isotope analyses.
709 Geochimica et Cosmochimica Acta 260, 275-291.
710 Tomioka, N., Tomeoka, K., Nakamura-Messenger, K., Sekine, T., 2007. Heating effects of
711 the matrix of experimentally shocked Murchison CM chondrite: Comparison with
712 micrometeorites. Meteoritics & Planetary Science, 42, 19-30.
713 Tonui, E., Zolensky, M., Hiroi, T., Nakamura, T., Lipschutz, M. E., Wang, M.-S., Okudaira,
714 K., 2014. Petrographic, chemical and spectroscopic evidence for thermal metamorphism in
715 carbonaceous chondrites I: CI and CM chondrites. Geochimica et Cosmochimica Acta
716 126, 284-306.
717 Travis, B.J., Schubert, G., 2005. Hydrothermal convection in carbonaceous chondrite parent
718 bodies. Earth and Planetary Science Letters, 240, 234-250.

719 Trigo-Rodriguez, J.M., Blum, J., 2009. Tensile strength as an indicator of the degree of
720 primitiveness of undifferentiated bodies. Planetary and Space Science, 57(2), 243-249.
721 Tyburczy, J. A., Xu, X., Ahrens, T. J., Epstein, S., 2001. Shock-induced devolatilization and
722 isotopic fractionation of H and C from Murchison meteorite: some implications for
723 planetary accretion. Earth and Planetary Science Letters, 192, 23-30.
724 Wetherill, G. W., 1975. Late heavy bombardment of the moon and terrestrial planets. In:
725 Lunar Science Conference, 6th, Houston, Tex., March 17-21, 1975, Proceedings. Volume
726 2. (A78-46668 21-91) New York, Pergamon Press, Inc., p. 1539-1561
727 Vacher L.G., Marrocchi Y., Verdier-Paoletti M., Villeneuve J. & Gounelle M., 2016. Inward
728 radial mixing of interstellar water ices in the solar protoplanetary disk. The Astrophysical
729 Journal Letters, 826, 1-6.
730 Vacher L.G., Marrocchi Y., Villeneuve J., Verdier-Paoletti M.J., Gounelle M., 2018.
731 Collisional and alteration history of the CM parent body. Geochimica et Cosmochimica
732 Acta 239, 213-234.
733 Vacher L.G., Piralla M., Gounelle M., Bizzarro M. & Marrocchi Y. (2019a). Thermal
734 evolution of hydrated asteroids inferred from oxygen isotopes. *The Astrophysical Journal*
735 *Letters 882*, L20.
736 Vacher L.G., Truche L. Faure F., Tissandier L., Mosser-Ruck R. & Marrocchi Y. (2019b).
737 Deciphering the conditions of tochilinite and cronstedtite formation in CM chondrites
738 from low temperature hydrothermal experiments. *Meteoritics & Planetary Science* 54,
739 1870-1889.
740 van Kooten, E.M., Nagashima, K., Kasama, T., Wampfler, S.F., Ramsey, J.P., Frimann, S.,
741 Balogh, Z.I., Schiller, M., Wielandt, D.P., Franchi, I.A., Jørgensen, J.K., 2017. A
742 divergent heritage for complex organics in Isheyevo lithic clasts. Geochimica et
743 Cosmochimica Acta 205, 119-148.

van Kooten, E.M., Cavalcante, L.L., Nagashima, K., Kasama, T., Balogh, Z.I., Peeters, Z., Hsiao, S.S.Y., Shang, H., Lee, D.C., Lee, T., Krot, A.N., 2018. Isotope record of mineralogical changes in a spectrum of aqueously altered CM chondrites. Geochimica et Cosmochimica Acta 237, 79-102.

Verdier-Paoletti, M. J., Marrocchi, Y., Avice, G., Roskosz, M., Gurenko, A., Gounelle, M., 2017. Oxygen isotope constraints on the alteration temperatures of CM chondrites. Earth Planetary Science Letters, 458, 273-281.

Verdier-Paoletti, M. J., Marrocchi, Y., Vacher, L. G., Gattacceca, J., Gurenko, A., Sonzogni, C., Gounelle M., 2019. Testing the genetic relationship between fluid alteration and brecciation in CM chondrites. Meteoritics & Planetary Science 54, 1692-1709.

Wiechert, U., Halliday, A.N., Lee, D.-C., Snyder, G.A., Taylor, L.A., Rumble, D., 2001. Oxygen Isotopes and the Moon-Forming Giant Impact. Science 294, 345-348.

Zolensky, M. E., 1997. Structural water in the Bench Crater chondrite returned from the Moon. Meteoritics & Planetary Science 32, 15-18

Zolensky, M. E., Weisberg, M. K., Buchanan, P. C., Mittlefehldt, D. W., 1996. Mineralogy of carbonaceous chondrite clasts in howardites, eucrites and the Moon. Meteoritics & Planetary Science 31, 518-537.

Zolensky, M.E., Mittlefehldt, D.W., Lipschutz, M.E., 1997. CM chondrites exhibit the complete petrologic range from type 2 to 1. Geochimica et Cosmochimica Acta 61, 5099-5115.

Zolensky, M. E., Buchanan, P., Le, L., Ross, D.K., J. Martinez J., 2019. Unusual tiny objects in your HED. Annual Meeting of the Meteoritical Society. Abstr. 6078.

Acknowledgements

We thank the NASA Johnson Space Center curatorial team for assistance in this project. This work was supported in part by NASA Lunar Science Institute contract NNA09DB33A and Solar System Exploration Research Virtual Institute contract NNA14AB07A (PI David A. Kring). Support also came from NASA Cosmochemistry grants to Scott Messenger and Mike Zolensky, and the UK Science and Technology Facilities Council (ST/M001253/1 and ST/P005225/1) and the Royal Society (RS/UF140190). We thank three anonymous reviewers and Prof. M. Lee for their insightful suggestions, and Prof. F. Moynier for editorial handling. This is LPI publication number XXXX. Jeff Taylor (Hawaii) first identified the Bench Crater meteorite and for that serendipitous discovery we are grateful.

Figure Captions

Figure 1. The Bench Crater meteorite**. (a)** Transmitted light optical image of Bench Crater meteorite showing a dark matrix and brown-coloured ferromagnesian silicate aggregates. **(b)** BSE image; the white arrow indicates the location where some matrix was extracted for NanoSIMS analysis; and see Figure S-4 for close up images. **(c)** False colour X-ray element composite map showing the mineralogical composition of the meteorite. Colour scheme indicated on the figure, where ferromagnesian silicate aggregates are cyan; matrix material is blue; apatite, calcite and dolomite are yellow; pyrrhotite, pentlandite and magnetite are red; ilmenite is pink; and the feldspathic agglutinate rim is white. **(d)** False colour X-ray element composite map. Colour scheme indicated on the figure, where apatite is cyan; calcite and dolomite are blue; pyrrhotite and pentlandite (S-bearing phases) are yellow; and magnetite is red.

Figure 2. BSE images of Bench Crater meteorite fabric showing a representative matrix region of the meteorite (a), and close up views of different ferro-magnesian aggregates (F-M Agg) (aqueously altered chondrule) comprised of intermediate phases (I-M phase), amorphous phases, ilmenite, apatite and pyrrhotite (Pyrr). Black linear features are fractures.

Figure 3. Mineralogy of the Bench Crater meteorite (area %) compared to that of CI, CM, CR, ungrouped C2 (C2-ung) and Adelaide carbonaceous chondrites. For Bench Crater, the normalised modal mineral proportions have been established from pixel analysis of X-ray composite phase maps of the whole section (see Supplementary Table S-2). Literature modal mineralogy (vol. %) data have been acquired using X-ray diffraction and are from Howard et al. (2010, 2011, 2015) and King et al. (2015, 2017) for CV, CI, CM, CR and C2-ung carbonaceous chondrites, and from Davy et al. (1978) for Adelaide meteorite.

Figure 4. BSE images of Bench Crater meteorite. **(a)** – **(d)** Close up of the thin (<100 μm) irregular vesicular glassy agglutinitic rim that partially coats about 10 % of the exterior of Bench Crater meteorite. Chemical analysis of the coat shows it to be feldspathic (Table S-3). Abbreviations are Ap for apatite, Mag for magnetite, F-M Agg for ferro-magnesian aggregate, and Pyrr for pyrrhotite.

Figure 5. Oxygen isotope composition of Bench Crater matrix, magnetite and carbonate, represented together with the bulk, matrix, magnetite and carbonate O isotope composition of CI and CM carbonaceous chondrite falls (data from Clayton and Mayeda, 1984, 1999; Rowe *et al.*,1994; Leshin *et al.*, 1997; Verdier-Paoletti *et al.*, 2017; Vacher *et al.*, 2018; Piralla *et al.*, 2020). CCAM and TFL stand for Carbonaceous Chondrite Anhydrous Mineral line and Terrestrial Fractionation Line, respectively. Note that the lunar oxygen isotope fractionation

line is identical to the TFL (e.g., Wiechert *et al.*, 2001). Carbonate T1 and T2 for Boriskino refers to carbonates formed before and after phyllosilicates, respectively (see Vacher *et al.*, 2018).

Figure 6. NanoSIMS maps of H, D, $^{12}C^{1}H$, ^{18}O and δD variations for Bench Crater Area 1. Intensities for H, D, $^{12}C^{1}H$, and ^{18}O correspond to counts per second, while δD values are given in permil normalised to VSMOW. Images have been smoothed by a moving $n \times n$ average where n = 3 and 9 pixels for intensity and δD maps, respectively, corresponding to ~235 and 705 nm spatial resolution.

Figure 7. Light isotope chemistry of the Bench Crater meteorite compared with the H, C and N isotope composition of a range of carbonaceous chondrites (data from Pearson et al., 2006 and Alexander et al., 2012) and the insoluble organic matter they host (data from Alexander et al., 2007), and of Apollo soil 12037 (Becker and Clayton, 1978; Kerridge *et al.,* 1978). Data for the two regions of Bench Crater measured in this study are linked by a dashed line, and uncertainties are at one sigma (Table 1). Organic rich nanoglobules from Tagish Lake meteorite (Nakumura-Messenger *et al.* 2006) typically plot off-scale as is the unusual organic rich CM chondrite Bells is indicated as having high $\delta^{15}N$ and δD compared with other CM group stones and ordinary chondrites. For comparison to comets we refer the reader to Figure 8.

Figure 8. (a) Hydrogen and **(b)** nitrogen isotope composition of the Bench Crater meteorite compared with different planetary materials (see Supplementary Information note S3 for literature sources). The δD value measured *in situ* for Murchison is shown in (a).

843

844 **Table 1.** Light isotope (H, C and N) compositions determined for fragments of the Bench
845 Crater and Murchison meteorites in this study and related literature measurements.

	δD (‰)	**± 2σ**	**$\delta^{13}C$ (‰)**	**± 2σ**	**$\delta^{15}N$ (‰)**	**± 2σ**
Murchison [a]	-117	± 98				
Murchison [b]			-1.61	± 0.19	52.7	± 0.31
Murchison [c]	-61.7	± 6.2	-2.87		45.57	
Bench Crater Area 1 [a]	-36	±40	-2	± 20	-27	± 20
Bench Crater Area 2 [a]	200	± 40	-23	± 20	-52	± 20
Bench Crater Area 3 [a]	-13	±18				
Bench Crater Area 4 [a]	35	±18				
Bench Crater C and N average (n. 2)			-13	± 30	-40	± 36
Soil 12037 (bulk)			-11.91[d]		-80.2[e]	
Soil 12037 (bulk)					-86 [f]	
Soil 12037 (High T steps)					-125 [f]	

846

847 [a] This study, determined by NanoSIMS analysis.

848 [b] Pearson *et al.* (2006)

849 [c] Alexander *et al.* (2012)

850 [d] Average of two reported values in Kerridge *et al.* (1978)

851 [e] Kerridge *et al.* (1978)

852 [f] Becker and Clayton (1978)

853 **Table 2.** Oxygen isotope results in phases within Bench Crater meteorite.

Phase	Analysis	$\delta^{18}O$ (‰)	2σ (‰)	$\delta^{17}O$ (‰)	2σ (‰)	$\Delta^{17}O$ (‰)	2σ (‰)
Silicates in aqueously altered chondrule	#1	14.58	1.28	6.51	0.54	-1.07	0.86
	#2	11.42	1.19	6.44	0.55	0.50	0.82
	#3	9.91	1.21	5.21	0.52	0.06	0.82
	#4	12.40	1.22	6.37	0.51	-0.08	0.82
	#5	11.63	1.19	6.36	0.51	0.32	0.80
	#6	12.79	1.19	6.42	0.51	-0.23	0.80
	#7	15.98	1.21	8.13	0.53	-0.18	0.82
	#8	16.79	1.16	8.30	0.52	-0.43	0.80
	#9	11.06	1.20	5.73	0.51	-0.02	0.80
Magnetite	#1	7.98	0.68	5.59	0.39	1.44	0.52
	#2	8.50	0.67	6.05	0.32	1.63	0.48
	#3	5.77	0.60	4.77	0.35	1.77	0.47
	#4	5.72	0.55	4.78	0.32	1.81	0.43
Carbonates	Dolomite#1	19.95	0.46	9.26	0.40	-1.12	0.47
	Calcite#1	12.76	0.54	6.39	0.38	-0.25	0.47

854

855

856

857

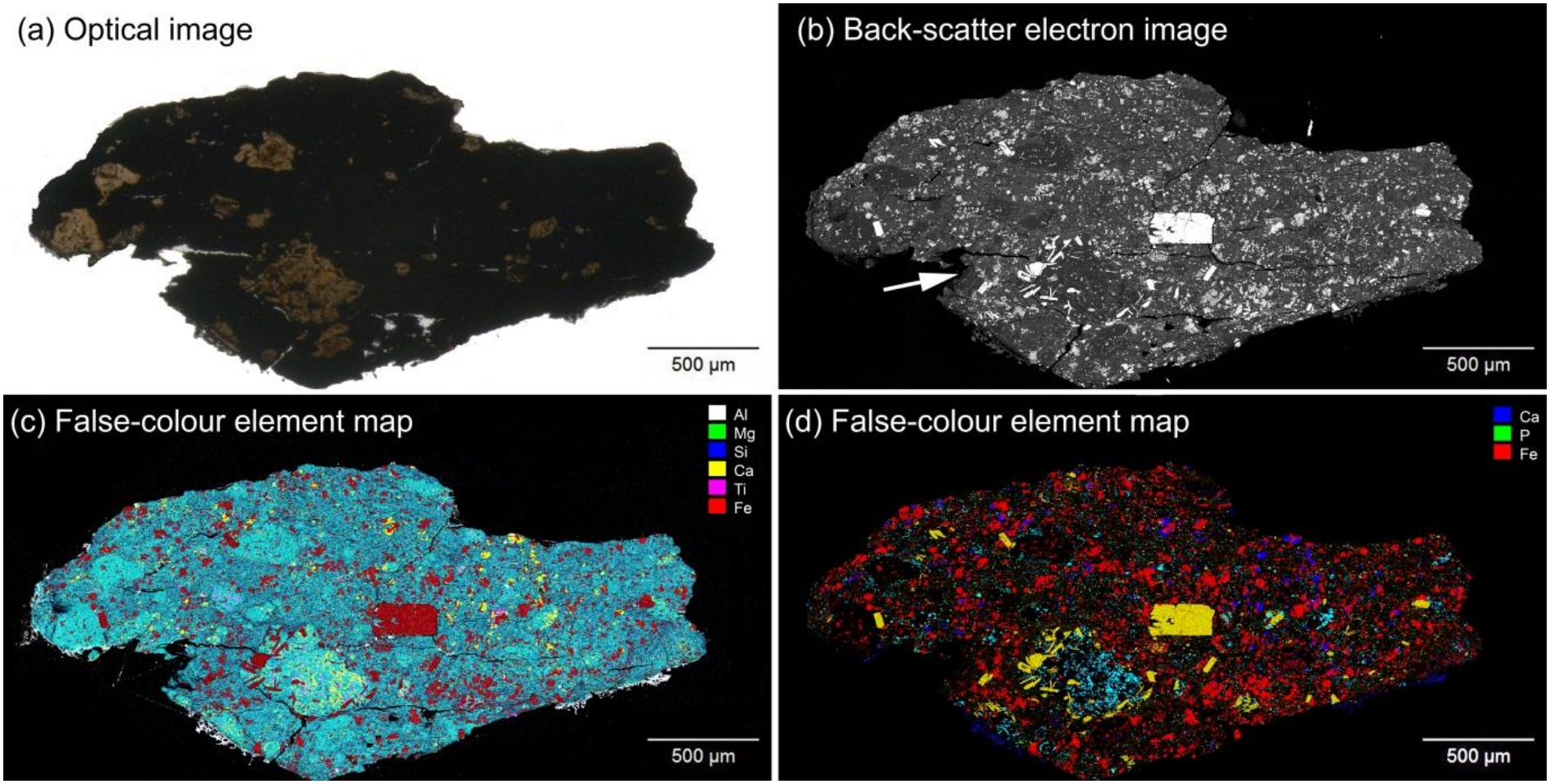

858

859 **Figure 1.**

860

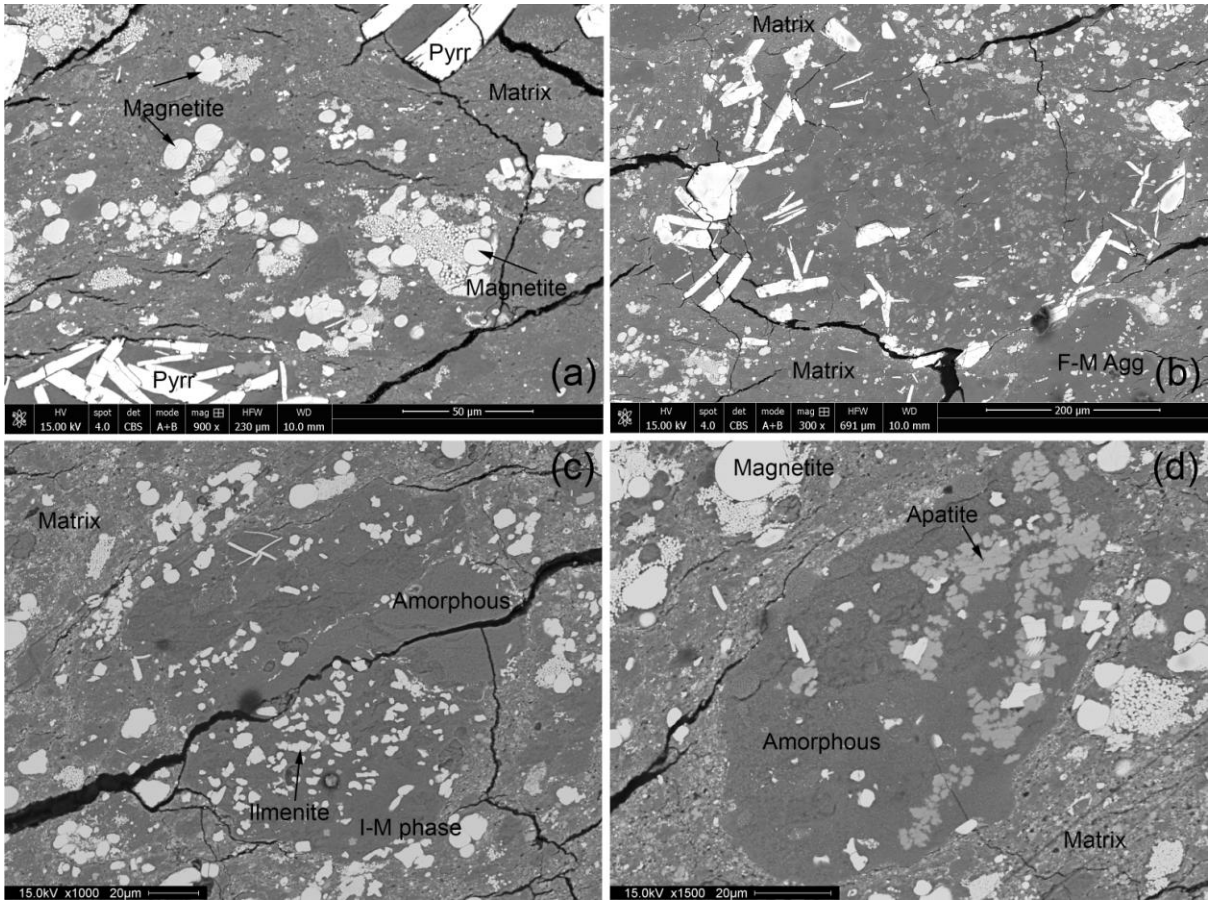
Pyrr
Matrix
Magnetite
Magnetite
Pyrr
(a)
HV 15.00 kV spot 4.0 det CBS mode A+B mag 900 x HFW 230 µm WD 10.0 mm 50 µm
Matrix
Matrix
F-M Agg
(b)
HV 15.00 kV spot 4.0 det CBS mode A+B mag 300 x HFW 691 µm WD 10.0 mm 200 µm
(c)
Matrix
Amorphous
Ilmenite
I-M phase
15.0kV x1000 20µm
Magnetite
(d)
Apatite
Amorphous
Matrix
15.0kV x1500 20µm

Figure 2.

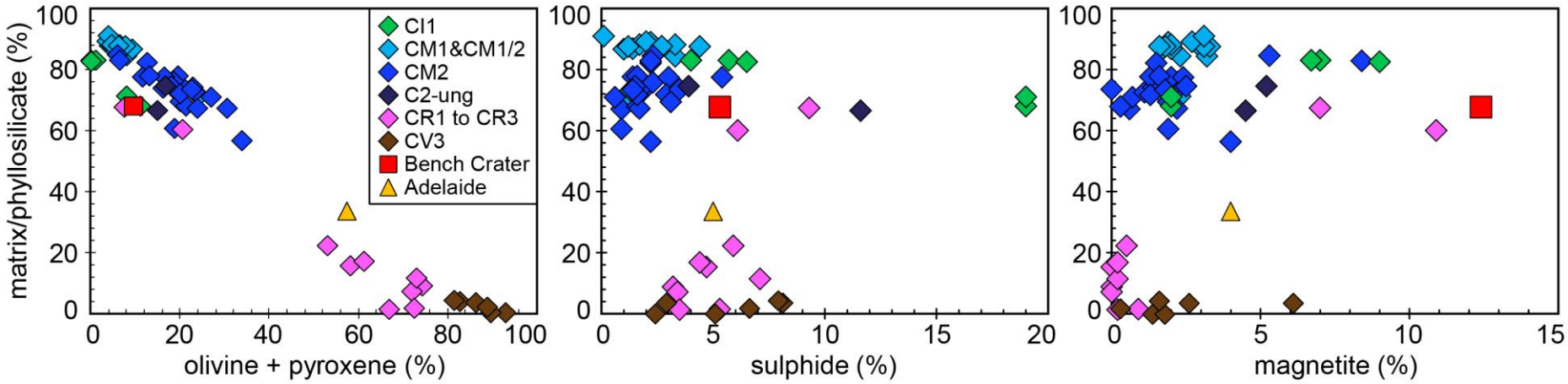

863

864 **Figure 3**.

865

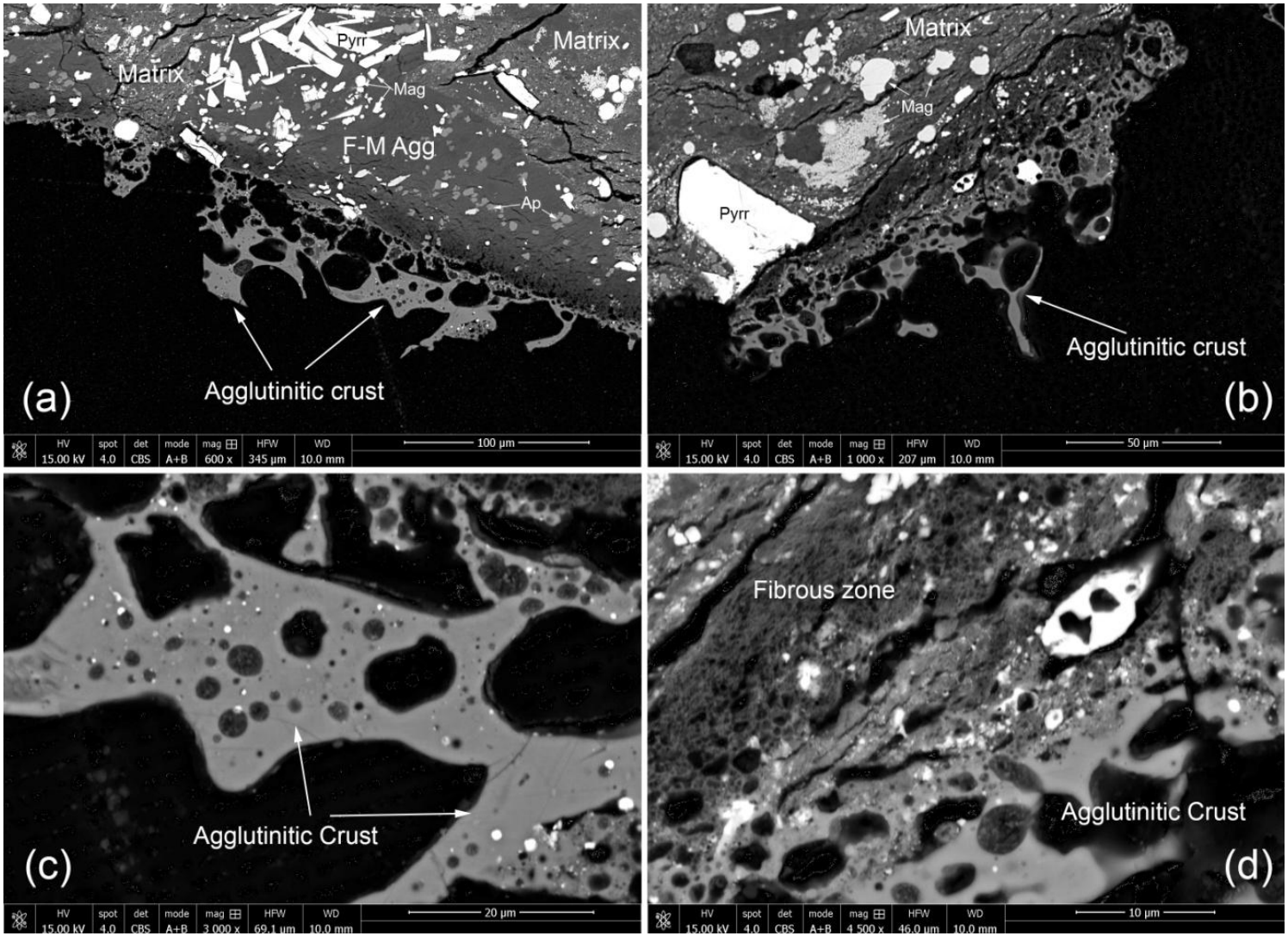
Matrix
Pyrr
Matrix
Mag
F-M Agg
Ap
Agglutinitic crust
(a)
HV 15.00 kV spot 4.0 det CBS mode A+B mag 600 x HFW 345 µm WD 10.0 mm 100 µm
Matrix
Mag
Pyrr
Agglutinitic crust
(b)
HV 15.00 kV spot 4.0 det CBS mode A+B mag 1 000 x HFW 207 µm WD 10.0 mm 50 µm
Agglutinitic Crust
(c)
HV 15.00 kV spot 4.0 det CBS mode A+B mag 3 000 x HFW 69.1 µm WD 10.0 mm 20 µm
Fibrous zone
Agglutinitic Crust
(d)
HV 15.00 kV spot 4.0 det CBS mode A+B mag 4 500 x HFW 46.0 µm WD 10.0 mm 10 µm

Figure 4.

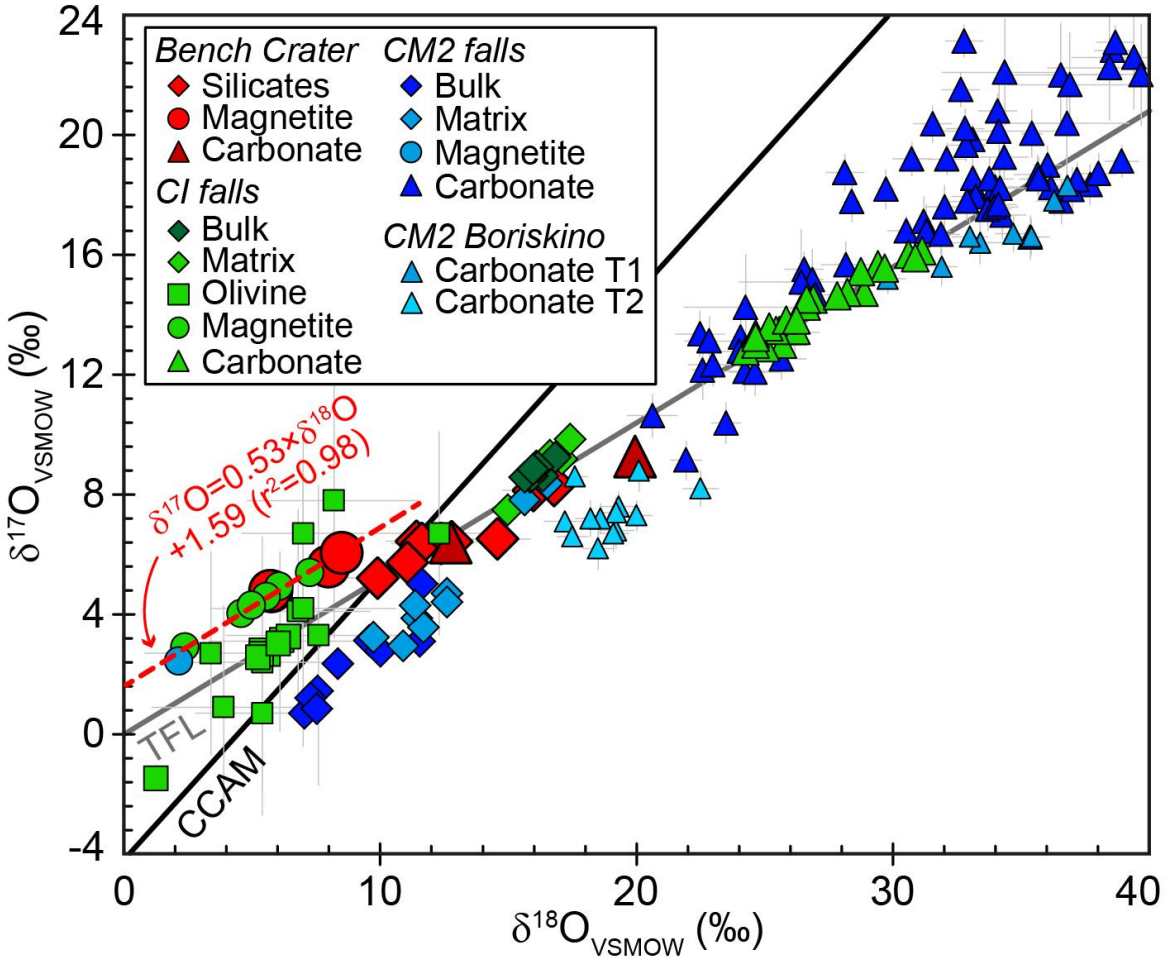
Bench Crater
Silicates
Magnetite
Carbonate
CI falls
Bulk
Matrix
Olivine
Magnetite
Carbonate
CM2 falls
Bulk
Matrix
Magnetite
Carbonate
CM2 Boriskino
Carbonate T1
Carbonate T2
δ17O=0.53xδ18O +1.59 (r2=0.98)
TFL
CCAM
δ17OVSMOW (‰)
δ18OVSMOW (‰)
24
20
16
12
8
4
0
-4
0
10
20
30
40

Figure 5.

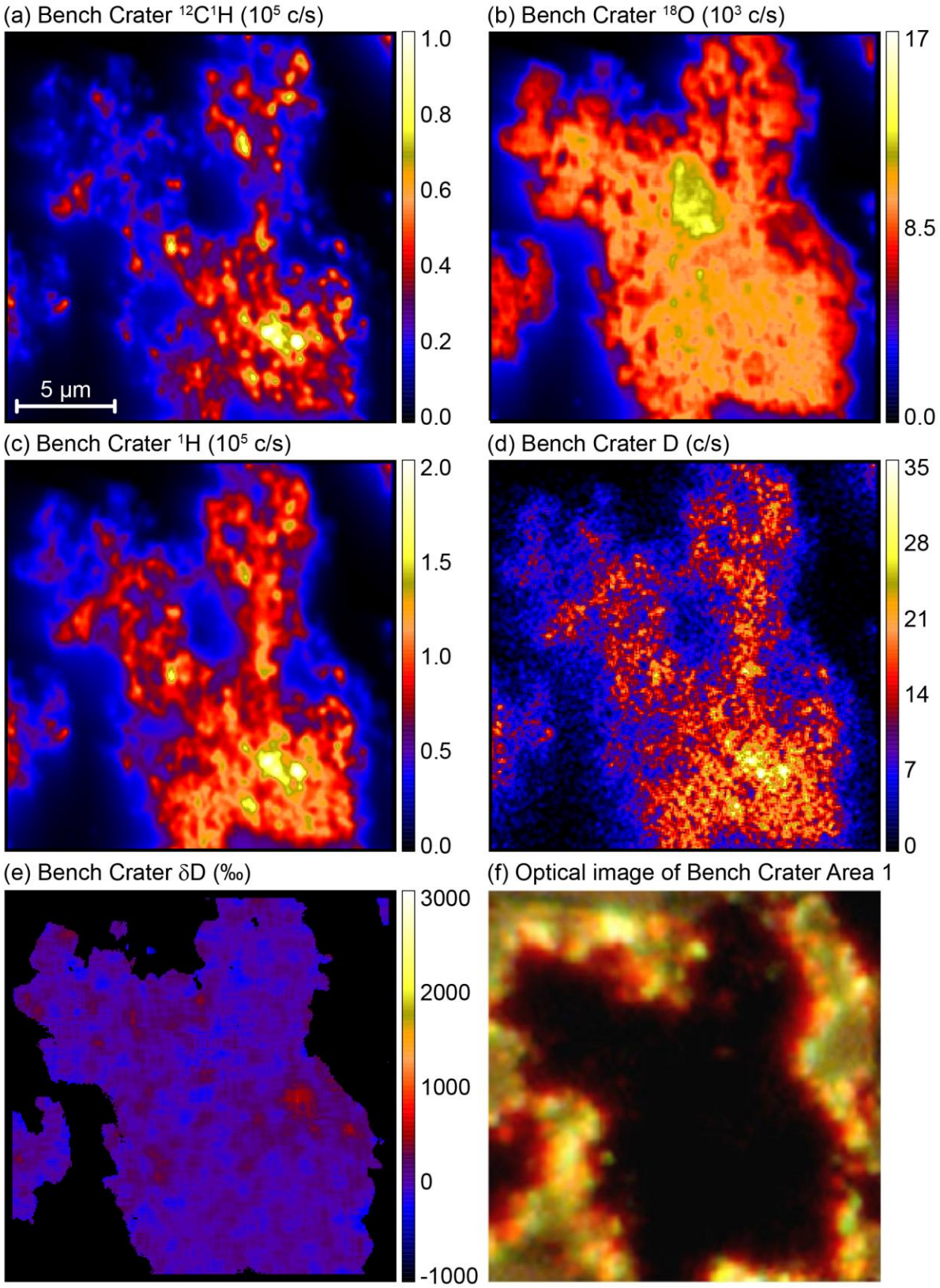

871

872 **Figure 6.**

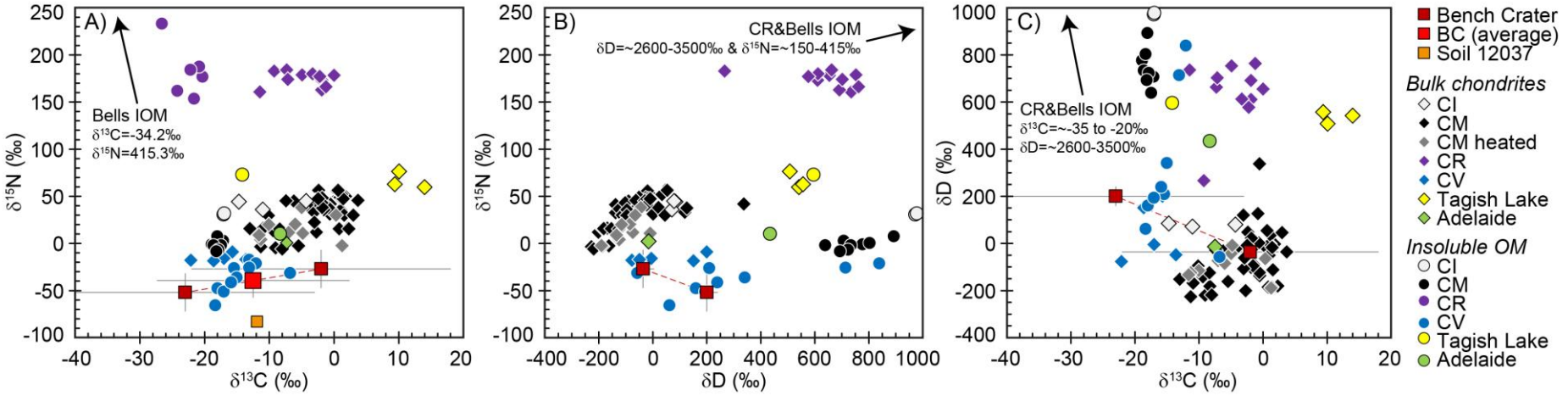

873

874 **Figure 7.**

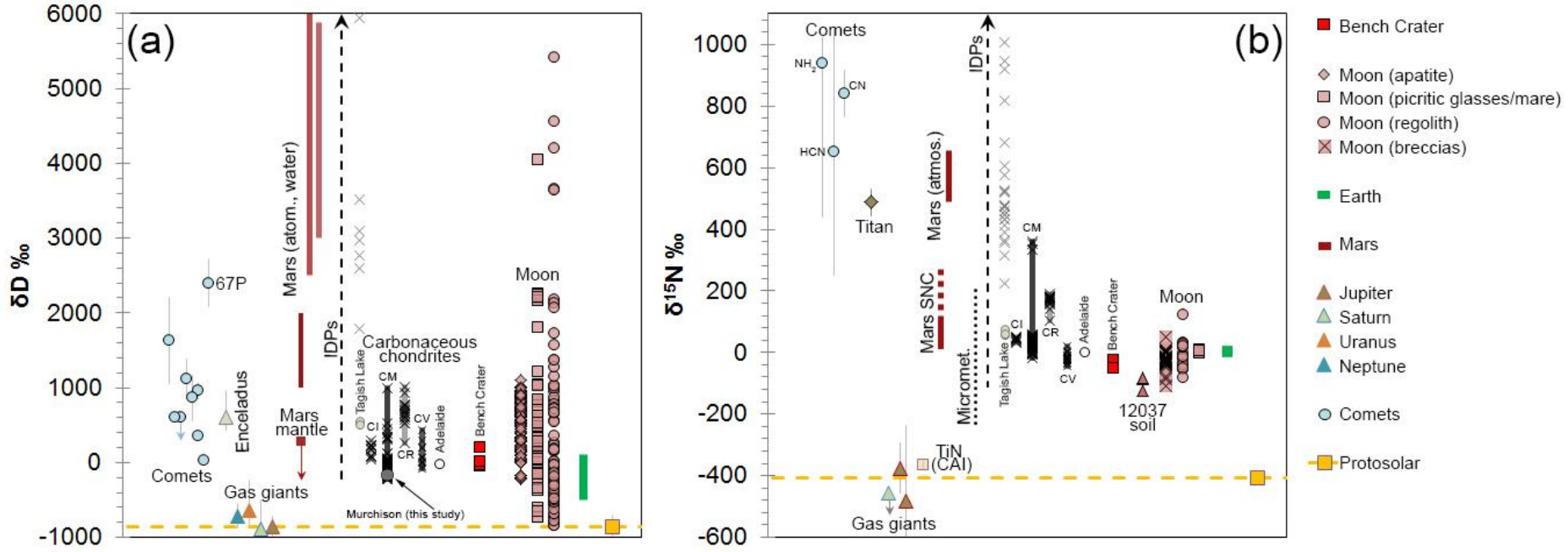

875

876 **Figure 8.**